A Novel High-Performance Consequent Pole Dual Rotor Permanent Magnet Vernier Machine

Arash Allahyari, Hossein Torkaman, *Senior Member, IEEE*

***Abstract*— This paper proposes a novel structure of consequent pole dual rotor permanent magnet vernier machine (CPDRVM). This structure consists of dual-sided stator in which windings are placed on the stator slots and magnets placed on the inner and outer rotor slots. Operation principles of the proposed VM carried out using flux modulation theory. The Finite Element analysis is utilized in order to evaluate the effect of magnet geometry on the produced torque and power factor. The motor characteristics and performance assessment are performed numerically. Furthermore, the parametric and sensitivity analysis are used to optimize the motor geometry. The proposed VM compared with PM machine and two conventional VMs. In this regard, performance indices such as flux, cogging torque, power factor, magnet volume, torque per magnet volume, Back-EMF, losses and efficiency profiles are calculated and compared. Results evidence better performance of the proposed structure. In fact, CPDRVM could produce higher torque density than conventional VMs. In addition, high power factor is reached for suggested topology.**

***Index Terms*— Dual air-gap, dual rotor consequent pole permanent-magnet machine, vernier machine, high torque density, finite element analysis, high power factor.**

NOMENCLATURE

Parameter	Description
PM	Permanent Magnet
CPDRVM	Consequent Pole Dual Rotor Vernier Machine
CPDS	Consequent Pole Dual Stator
VM	Vernier Machine
VPMSM	Vernier Permanent Magnet synchronous Machine
DSSA	Dual Stator Spoke array
DSSAVM	Dual Stator Spoke array Vernier Machine
MMF	Magnetomotive Force
FEM	Finite Element Method
TPMV (pu)	Torque per Magnet Volume
Back-EMF	Back Electromagnetic Force
PF	Power Factor

I. INTRODUCTION

Due to wide usage range of direct-drive applications such as electric propulsion, wind and wave energy generation and because, mechanical gearboxes are heavy and require high maintenance, researchers concentrated on the development of electrical machines that can generate high torque density at low speed rotation without the necessity for a mechanical gearbox [1]. Various permanent magnet (PM) machines suggested in order to achieve high torque at low speed such as, flux switching machine [2], flux reversal machine [3], axial flux machines [4], double salient machine [5-7] and vernier machine (VM). Among different type of electrical machines, Vernier PM Machines proposed because of their capability to generate high torque density at low speed, which is achieved by magnetic gear effect in the air gap. Hence, VMs are considered as great candidates to generate high torque at low speed. Therefore, understanding operation principles of magnetic gears and VMs and their relationship would be essential. In addition, field modulation theory for electrical machines explained carefully in [8] with concentration on new topologies of electrical machines. Operation principles of VMs and justification of higher torque generation capability included in [9], reveals magnetic gearing effect in VMs. Considering above mentioned papers proposed and studied VMs could be included in one of these groups, single air-gap, dual air-gap and usage of various magnet topologies.

Significant drawback of VMs is low power factor (PF) in which could cause a higher cost of drive circuit. Regarding a solution for achievement of higher PF, researchers proposed different structures such as spoke type magnets, surface mounted magnets on stator and rotor, consequent pole and halbach dual side topologies [10,11]. In addition, an axial flux dual rotor VM suggested in [12] that did not display promising results. In [13]-[15] researchers proposed two dual stator structures of VM with spoke type and halbach magnets to achieve better performance and high PF. Utilizing enhanced flux modulation effect, [16] proposed a novel structure of single air-gap VM with spoke type magnets on the rotor.

[17] Proposed high PF VM using structure with coil pitch of two slot pitches. Cost and availability of materials is an inevitable factor for every PM machine. In [18] proposes a structure of VM that does not include magnets. Operation of a VM as a generator for different application and remote energy generation studied in [20, 21]. In [22] authors conduct a comparison between integral and fractional slot VMs.

Among proposed VMs, dual stator spoke array vernier machine (DSSAVM) has an advantage of higher PF with high torque production capability, which was significant drawback of conventional VMs. Comprehensive explanation of different topologies of DSSAVM, scaling, performance and demagnetization analysis is performed [23,24]. Demagnetization is a major drawback in most of PM machines, in which [25] considers demagnetization phenomena of VMs. A new topology of DSSAVM that utilizes alternating rotor leakage flux blocking design proposed in [26].

In this regard, VMs have been considered because of their high torque density at low speed. But, low PF is a major drawback in VMs in which this paper proposes a novel structure of VM, namely as consequent pole dual rotor vernier machine (CPDRVM), that can generate considerable high torque density and achieve high PF simultanesouly. And the other advantage of proposed CPDRVMs is utilizing lower magnet volume in comparison with typical vernier permanent magnet machines. Novelty of proposed structure is to utilize dual rotor and single stator strucutre with two windings on the stator.

*Corresponding author: h_torkaman@sbu.ac.ir

Accordingly, paper context organized as, section II explains structure of the typical VMs and proposed CPDRVMs. The operation principles of the machine are described in section III. Results of electromagnetic analysis of the proposed CPDRVMs are explained in section IV for calculation of Back-EMF, torque and PF. Section V is dedicated to sensitivity analysis in order to optimize performance of CPDRVMs considering TPMV (pu), PF and effect of machine dimensions using introduced variables. Section VI completes paper by a brief explanation of the obtained results.

II. PROPOSED CPDRVM TOPOLOGY

Typical VMs and proposed CPDRVM are depicted in Fig. 1 and Fig. 2 respectively. Three typical VMs displayed in Fig. 1 are compared with proposed VM displayed in Fig. 2.

Model A consisted of 24 slots (CPDRVM-A) and Model B consisted of 48 stator slots (CPDRVM-B). Inner and outer rotors of Model A and Model B have 22 and 44 slots respectively in which these slots have been filled with magnets (Fig. 2). Moreover, magnetization direction of inner and outer rotor magnets is radial (+R).

Significant difference between typical and proposed machines is that the proposed VM have two rotors while typical VMs has only one rotor. In addition, unlike the other types of the VMs, CPDRVM has a double side stator to encounter with inner and outer rotors. Moreover, two types of CPDRVM introduced in order to elaborate capabilities of proposed CPDRVM.

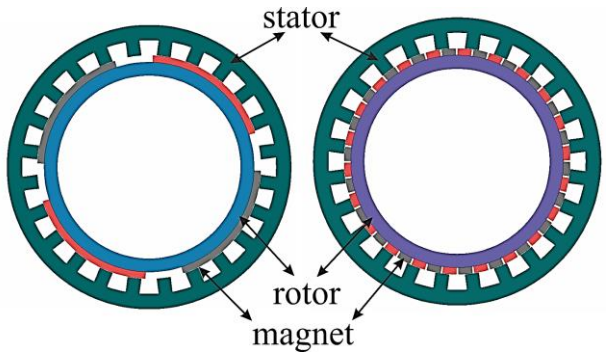

(a) Four-pole PM machine (b) Single Sided VM

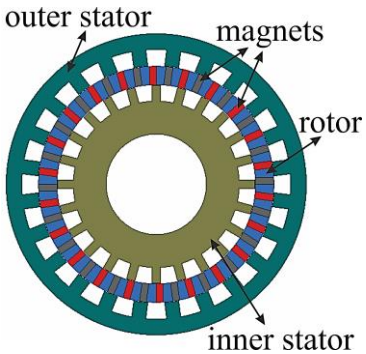

(c) DSSAVM

Fig. 1. Typical machines [15]

In this regard, DSSAVM has 44 poles on rotor and 24 poles on the inner and outer stators. Proposed structure consisted of laminated stator, which is uniformly made up 24 poles on the stator and 22 consequent poles on the inner for the CPDRVM-A, and 48 poles on the stator and 44 consequent poles on the inner and outer rotor for the CPDRVM-B. From the advantages of the presented motor, one can mention the amount of utilized magnets and cost that will be evaluated in comparison study. Inner and outer stator windings connected together in series. Windings connection configuration of the stator depicted in Fig. 4.

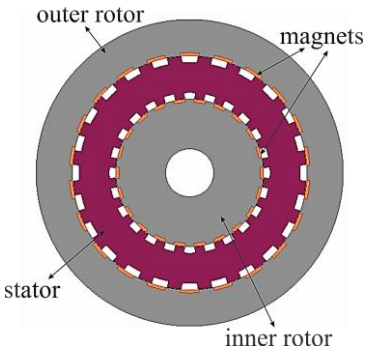

(a) CPDRVM-A

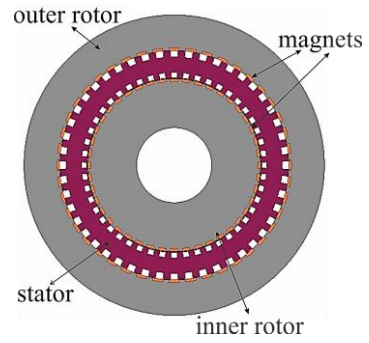

(b) CPDRVM-B

Fig. 2. Proposed CPDRVM in two models

In Fig. 3, the three-dimensional (3D) exploded model of motor is illustrated. According to the 3D disassembled model of the CPDRVM machine, a two-dimensional (2D) model can be presented to better understand the operational principles of this structure.

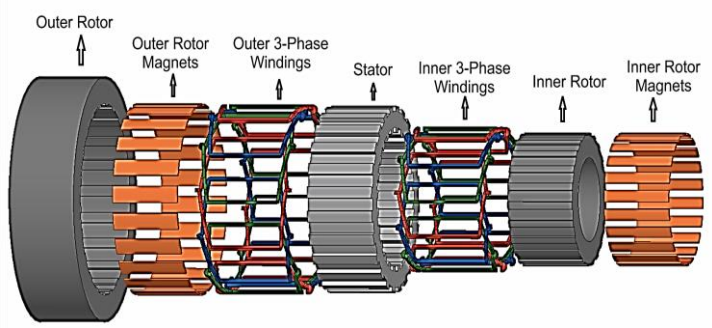

Fig. 3. The 3D exploded view of presented CPDRVM

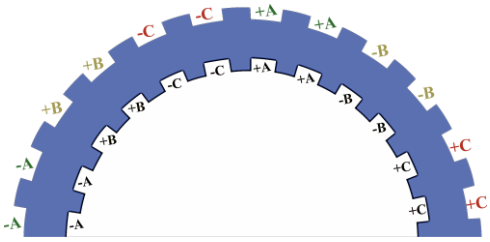

Fig. 4. Winding configuration of CPDRVM located on the stator

III. Analysis and Principles of the CPDRVM Operation

VMs are classified as a flux modulating machine. Due to magnetic gearing effect, rotation speed is much smaller than that of electromagnetic field. Generally, a conventional VM is consisted of a single stator and surface mounted PM rotor (Fig. 1b). Therefore, analysis of one of air-gap permeance caused by permanent magnet MMF and stator windings in which would eventually generates torque, will be sufficient for understanding operation principle of a VM. This analysis is performed utilizing the method introduced in [15] and [23].

Table I: Parameter Definition

Parameter	Unit	Description
θ_s	Deg.	mechanical angle on the stator
S_s	-	Number of stator slots
P_r	-	Number of rotor poles
P_s	-	Number of stator poles
ω	rad/s	Electrical angular velocity
B_g	T	Harmonic of the modulated flux density
F_{PMg}	A	PM MMF
K_1	-	Winding factor
I_{pk}	A	Peak input current
C_p	-	Number of parallel circuits
γ	Deg.	Current phase shift angle
N_t	-	Number of turns
W_{stator}	mm	Stator width
W_{orm}	mm	Width of outer rotor magnet
W_{irm}	mm	Width of inner rotor magnet
θ_{orm}	Deg.	Arc of outer rotor magnet
θ_{irm}	Deg.	Arc of inner rotor magnet

The magnetomotive force (MMF) developed by PMs can be expressed by in the form of Fourier series as (1), where P_r is the number of rotor poles. Furthermore, the air-gap permeance of the open slot-tooth structure is described by (2) [23]. The design parameters are defined in Table I.

$$F_{PMg}(\theta_s\, t) = \sum_{h=odd} F_{PMg} cos(hP_r\theta_s - h\omega t) \quad (1)$$

$$\Lambda(\theta_s) = \Lambda_0 + \sum_{h=odd} \Lambda_h cos(hS_s\theta_s) \quad (2)$$

where θ_s, ω, S_s and P_r are described at Table I. The air-gap flux density B_g is calculated by multiplication of (1) and (2).

$$B_g(\theta_s\ \theta_r) = \Lambda(\theta_s)F_{PMg}(\theta_s t) \quad (3)$$

Significant difference between the proposed CPDRVM and DSSAVM is that in DSSA air-gap permeance as a result of stator flux modulation has harmonics in which they are multiplied by $P_r/2$. However, in CPDRVM, harmonics of the air-gap permeance of stator flux modulation are multiplied by P_r . Fundamental harmonic of the air-gap modulated flux density wave (B_g) which is production of the air-gap permeance and the air-gap MMF calculated in (4). In addition, fundamental stator MMF wave produced by a three-phase balanced stator current excitation in the air-gap expressed in (5).

$$B_g = F_{pmg1}\left[\Lambda_0\cos(P_r(\theta_s) + \omega t) + \frac{\Lambda_1}{2}\cos\big((P_r + S_s)\theta_s - \omega t\big) + \frac{\Lambda_1}{2}\cos\big((P_r - S_s)\theta_s + \omega t\big)\right] \quad (4)$$

$$F_{esg1} = \frac{3}{2}\frac{4}{\pi}\frac{K_1 N_t I_{pk}}{C_p P_s}\cos\left(\frac{P_s}{2}\theta_s - (\omega_e t - \gamma)\right) \quad (5)$$

where K_1, N_t, I_{pk}, C_p, P_s, γ are also described in Table II.

In order to generate positive average torque, frequencies of the rotor modulated wave and stator MMF wave must be equal. This equality could occur in other frequencies of air-gap flux density rather than fundamental shown in (4) too.

$$\frac{P_s}{2} = P_r \pm S_s \quad (6)$$

Equation (6) shows that both '+' and '−' could produce torque. However, according to [15] '−' state produces higher torque. Therefore, state '−' is the considered (7).

$$P_s/2 = P_r - S_s \quad (7)$$

It should be considered that (7) shows only one equality for torque production. However, there could other coupling for other frequencies of air-gap permeance and stator MMF wave that eventually would produce higher torque density. Equation (8) shows another equality for torque generation in which l is a non-zero integer number.

$$S_s = 6l(P_s/2) \quad (8)$$

Equation (8) shows that six multiples of initial is also collaborate in torque generation in which verified by air gap harmonics displayed in Fig. 9.

IV. Electromagnetic Analysis and Comparison Study

After the initial design of the machine, the initial modeling and then the structural optimization, the optimized machines are evaluated using numerical analysis. In this regard, proposed motors characteristics are obtained and analyzed using FEM. Typical machines are a four-pole PM machine, a dual stator spoke type (DSSA) VM and a single-sided VM. Significantly, a fair comparison among typical and proposed machines regarding produced Back-EMF, torque per magnet volume (TPMV) and PF are performed. In addition, same dimension constraints considered such as inner and outer dimensions, stack length, air-gap length, phase turns and current density. Proposed CPDRVM structure has windings placed on the stator slots and inner and outer rotor have consequent pole magnets.

Dimensions of the typical and proposed VMs are included in Table II and Table III respectively. In order to compare typical and proposed VMs, dimensions could be found in [15] utilized as the base design in order to have fair comparison. Fig. 5 displays considered variables including geometry of consequent pole inner and outer rotor magnets and stator width.

Table II : DIMENSIONS OF TYPICAL VMs

Parameter	Unit	DSSA	Single – Sided VPM	Four-Pole PM
Outer rotor inner diameter	mm	490	490	490
Outer stator outer diameter	mm	620	620	620
Inner stator inner diameter	mm	340	--	--
Inner stator outer diameter	mm	407	--	--
Spoke array magnet width	mm	14	--	--
Spoke array magnet height	mm	38	--	--
Stack Length	mm	50	50	50
Stator Poles, P_s	-	4	4	4
Rotor Poles, P_r	-	44	44	4
Stator Slots, S_s	-	24	24	24
Inner air-gap	mm	1.5	1.5	1.5
outer air-gap	mm	1.5	--	--
Magnet outer diameter	mm	--	486	486
Rotor inside diameter	mm	--	400	400
Rotor inside diameter	mm	--	458	458

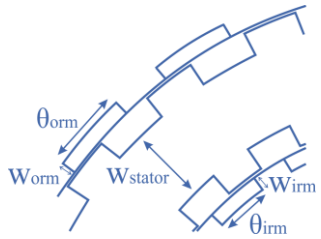

Fig. 5. Proposed CPDRVM dimension variables

Table III: Dimensions of the proposed VMs

Parameter	Unit	CPDRVM Model A	CPDRVM Model B
Outer rotor inner diameter	mm	489	489
Outer rotor outer diameter	mm	640	620
Inner rotor outer diameter	mm	367	367
Stack Length	mm	50	50
Stator Slots, S_s	-	24	48
Rotor Poles, P_r	-	22	44
Inner and outer air-gap	mm	1.5/1.5	1.5/1.5
Magnet Type	--	NdFe35	NdFe35
W_{rotor}	mm	40	30
W_{orm}	mm	5	3
W_{irm}	mm	5	3
θ_{orm}	Deg.	10	5
θ_{irm}	Deg.	10	5

A. Back-EMF and no-load flux lines

Back-EMF is an important property of the PM machines. It has been shown that a VM can produce much higher Back-EMF using other harmonics of air-gap flux density.

Proposed machines are modeled by FEM according to the dimensions of machines in Tables II and III. Back-EMF of the CPDRVM and typical machines calculated in a no-load condition which, its effective values (*rms*) shown in Table IV as well as magnet volume usage. Calculation of Back-EMF per magnet volume is because of dissimilar usage of magnet volume in typical and CPDRVMs. Among all machines, CPDRVM-A generates highest Back-EMF per magnet volume, which is almost 1.44 times bigger than DSSA and 2.4 times bigger than Single-Sided VPM. Whereas CPDRVM-B generates 1.19 times higher Back-EMF than DSSAVM.

As shown in Table IV, the amount of magnet volume used in the new topology, CPDRVM-A is 50%, 55% and 65% lower than PM, VM and DSSAVM, respectively. In addition, utilized magnet volume in CPDRVM-B is 50% lower than CPDRVM-A. It means that the cost of magnet in these structures has been decreased vitally, that is very important for producers and manufacturers.

Table IV: BACK EMF VALUES

Parameter (at 30 rpm)	Back EMF (V_{RMS})	Magnet volume (cm^3)	Back-EMF per magnet volume(V/cm^3)
PM machine	9.04	807.319	0.011
Single-Sided VPM	38.5	888.051	0.043
DSSAVM	84.5	1171.16	0.072
CPDRVM-A	44.77	401.25	0.111
CPDRVM-B	26.85	197.20	0.13

In order to maximize induced flux in DSSA, inner stator has half pitch displacement compared to the outer stator teeth [15]. Whereas, maximum Back-EMF of the proposed CPDRVM is achieved when inner and outer rotors are aligned (Fig. 2). Half pitch displacement of inner and outer stator of proposed CPDRVM will cause phase displacement in the windings induced voltage that could cause higher cogging torque.

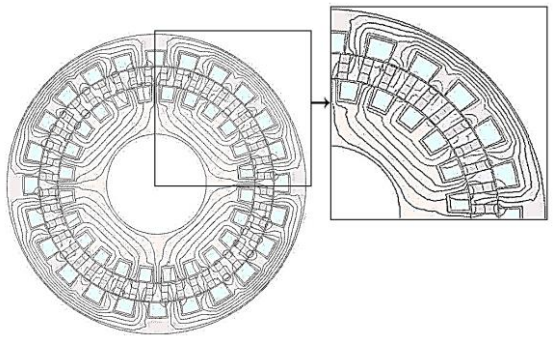

Fig. 6. Flux distribution of DSSAVM at no load [15]

Fig. 6 and Fig. 7 show the flux distribution of DSSAVM and CPDRVMs respectively. There are more flux paths in DSSA that is because; magnet usage of DSSA is almost three times Model A and 6 times Model B. However, CPDRVM-A and CPDRVM-B could generate 1.54 and 1.8 times higher Back-EMF per magnet volume than DSSAVM.

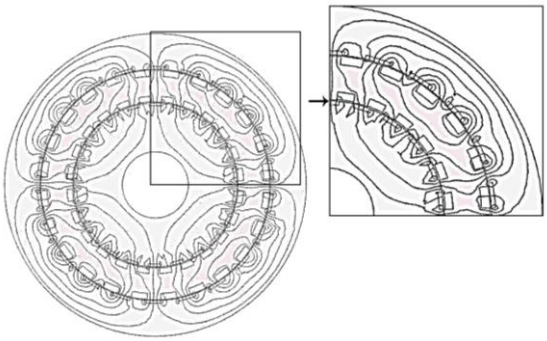

(a) CPDRVM-A

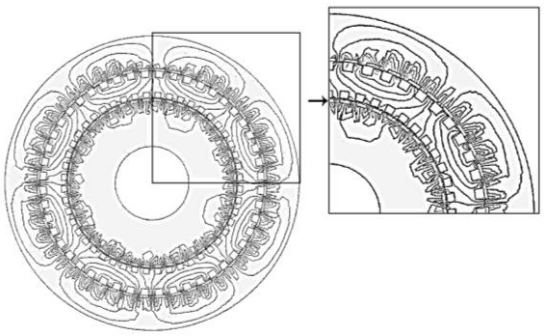

(b) CPDRVM-B

Fig. 7. Flux distribution at no-load

B. *Air-gap flux density*

Fig. 8 illustrates the air-gap flux density distribution at no-load test. In addition, Fig. 9 displays harmonics of the no-load flux density distribution in the motor Fig. 9 demonstrates that different harmonics contributed for Back-EMF generation resulted from the magnets of inner and outer rotors.

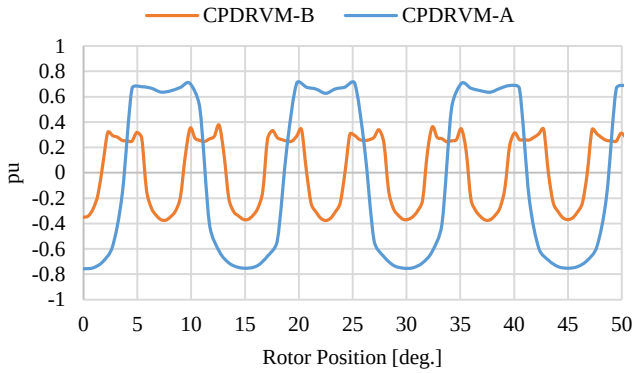

Fig. 8. No-load air-gap flux density distribution in CPDRVM

C. *Fundamental harmonics*

Considering the equations explained in section III; the fundamental harmonic of the air-gap flux density plays major rule in torque generation. In fact, the greater the amplitude of this component is the greater torque could be produced utilizing same input current. In addition, the VM has two working magnetic field components, which are named as fundamental and harmonic fields, respectively. As shown in Fig. 9 the low-order harmonics have been transmitted to high order in CPDRVM-B respect to the CPDRVM-A. Therefore, their impact on the fundamental component is less.

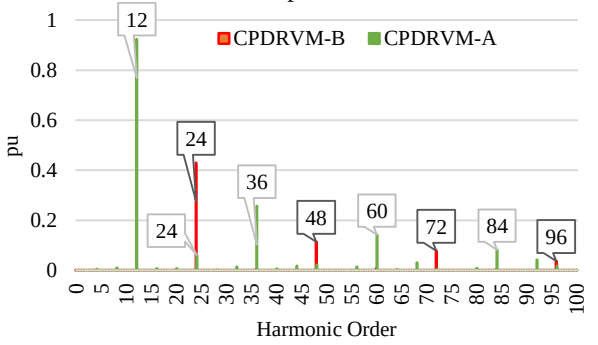

Fig. 9. Proposed CPDRVMs harmonic components of air-gap flux density distribution

D. *Flux density of DSSAVM and proposed VMs at loaded condition*

Fig. 10 and Fig. 11 show flux density distribution of the DSSAVM and proposed VMs respectively at loading condition. It should be mentioned that current desnity in machines are considered carefully to be same. In fact, input current is 20 A in all three machines. However, since CPDRVM-B has 48 slots, number of coil turns is half of the CPDRVM-A. Maximum flux desnisty of DSSAVM is 1.83T which is higher than proposed CPDRVM-A with 1.7T and CPDRVM-B with 1.6T. In addition, higher flux density could mean higher operation temperature and higher core loss. Furthermore, higher operation temperture could cause demagnetization problem for DSSAVM. Therefore, there is necessity for more research over demagnetization problem.

In this regard, CPDRVM-B has the lowest core flux density among VMs and lower core losses in comparison with CPDRVM-A and DSSAVM. It should be stated that turn per phase and electrical loading are same in the mentioned three models.

By considering results it can claimed that propsed CPDRVM could work in higher input currents and generate more torque. However, careful assessment of the proposed design needed for smooth operation of the machine.

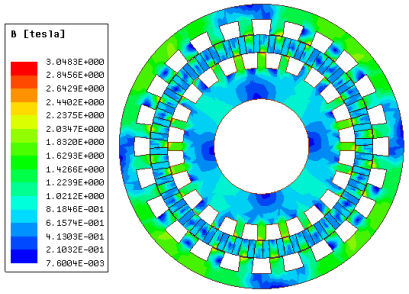

Fig. 10. Flux density distribution of DSSAVM

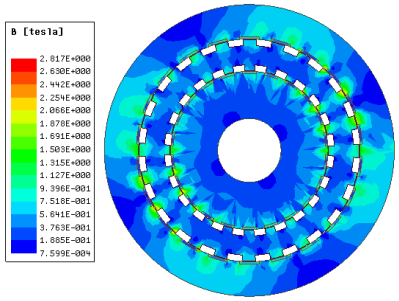

(a) CPDRVM-A

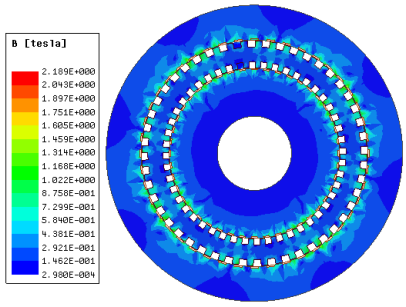

(b) CPDRVM-B

Fig. 11. Flux density distribution of proposed VMs in loading condition

E. *The Cogging Torque of CPDRVMs*

Cogging torque generated by the interaction of magnets. Cogging torque could be seen in the produced torque like a noise. The cogging torque is not a function of the speed. It is only a function of the structural dimensions including the stator and rotor slot-opening width, the shape, position and thickness of the magnets. The cogging torque often has a large value in structures with a modular or segmented rotor, which causes the output torque ripple. In this structure, the cogging torque has a small value. It is due to the small width of the stator slot-opening and also the small overlap between the rotor poles and the stator poles.

Fig. 12 shows cogging torque of the inner and outer rotor for CPDRVM-A and CPDRVM-B separately. Fig. 12 demonstrates that the outer rotor faces higher cogging torque. In addition, the amplitude of cogging torque in CPDRVM-A is higher than CPDRVM-B. Besides, cogging torque could be seen in output torque. In this regard, Fig. 15 shows that CPDRVM-A has a higher torque ripple.

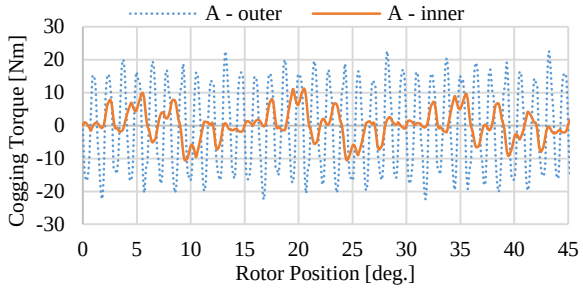

(a)

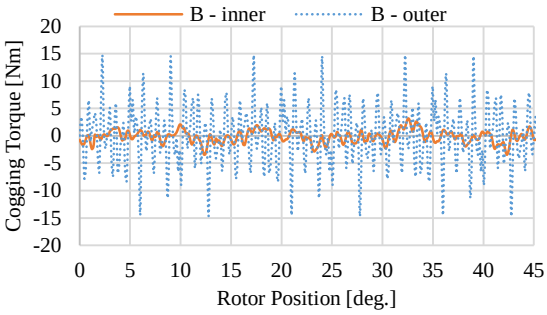

(b)

Fig. 12. Cogging torque of the CPDRVMs for inner and outer rotors in: (a) model A, (b) model B.

V. SENSITIVITY ANALYSIS AND PERFORMANCE INDICES DISCUSSION

A. *Optimization and sensitivity analysis*

In order to investigate performance and capabilities of the proposed CPDRVMs, the sensitivity and optimization analysis are considered. Optimization process consisted of two significant factors, TPMV and PF [27-29]. In fact, study in this section considers finding optimum values of magnet geometry (magnet arc and width) evaluating effect of these variables on the TMPV and PF. As demonstrated in Fig. 13 and Fig. 14. It should be mentioned that same values for magnet arc, θ_{orm} and θ_{irm}, which defined as inner and outer rotor magnets are considered. In addition, inner and outer magnet width, W_{orm} and W_{irm}, also has same values.

The results of Fig. 13a show that higher magnet arc means higher power factor with the cost of TPMV. In fact, proposed CPDRVM-A reaches TPMV value of 2.4 with 0.77 PF. In addition, Model A could reach 0.96 PF but with TPMV value of 0.83. Therefore, it is a tradeoff between TPMV and PF.

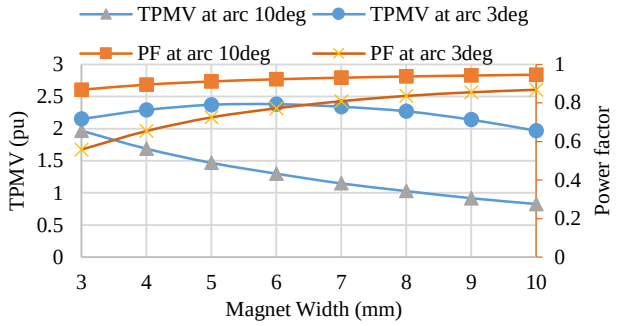

(a)

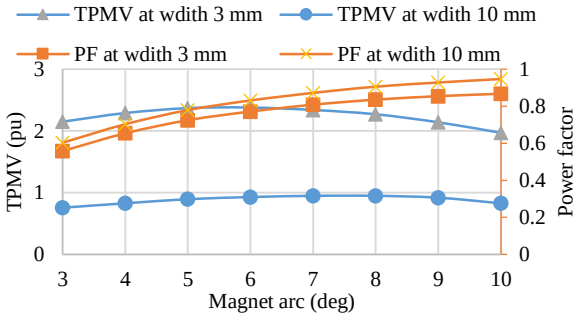

(b)

Fig. 13. PF and TPMV for CPDRVM-A (a) versus magnet width variations, and (b) versus magnet arc variations

Results displayed in Fig. 13b show that with increase of magnet arc PF increases dramatically. However, TPMV is another story in which it increases until 6 degrees' magnet arc then decreases. Moreover, other values of magnet arc and width will result in values that will place TPMV and PF values between shown waveforms of Fig. 13. Therefore, utilizing results shown in Fig. 13, magnet arc and width selected to be 10 degrees and 5 mm that makes values of TPMV and PF equal to 1.47 and 0.91 respectively to be the optimized CPDRVM-A.

Fig. 14 demonstrates parametric analysis of CPDRVM-B. As illustrated in Fig. 14a and Fig. 14b, with increase of magnet width, TPMV decreases and value of TPMV is almost same when magnet arc is equal to 2 and 4 degrees. However, PF is much higher when magnet arc is equal to 4 degrees. Moreover, Maximum value of TPMV is 1.85 with PF equal to 0.88 and maximum value of PF is 0.92 with TPMV equal to 0.77. Therefore, maximum TPMV and PF reached when magnet arc and magnet width are 3 and 4 degrees respectively. In this regard, magnet width and arc equal to 3 mm and 4 degrees has been chosen as optimized CPDRVM-B.

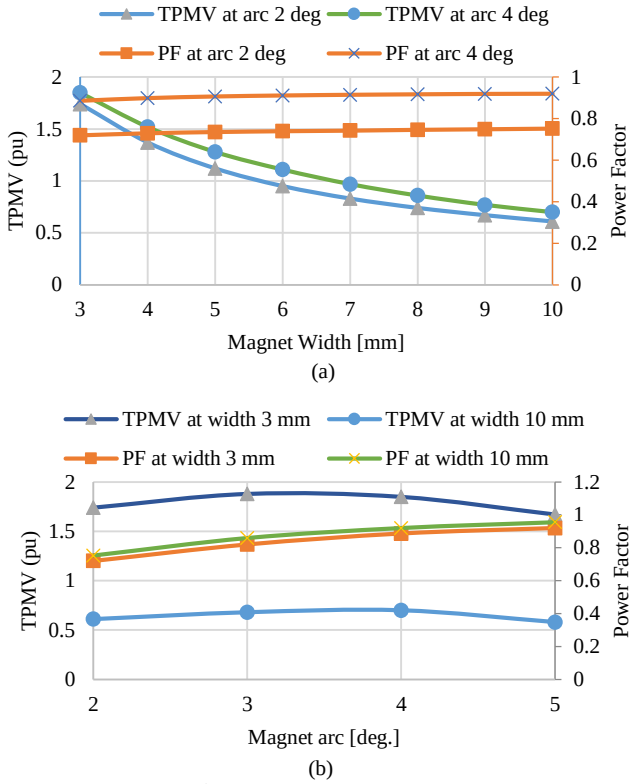

Fig. 14. PF and TPMV for CPDRVM-B (a) versus magnet width variations, and (b) versus magnet arc variations

Principle reason of declining and increasing both torque and power factor while changing geometry (width and arc) of magnets is change of flux distribution in the rotor, stator and airgap of the machine. Magnet geometry is the key factor of the proposed Vernier machine. In fact, flux produced by magnets could cancel or strength each other considering flux path produced by them. In this regard, voltage harmonics are changing considering flux generated by different geometry of magnets. These harmonics can strengthen the principle harmonic or cancel it. Optimized point is the point that harmonics amplitude participates with the principle harmonic in order to generate higher torque.

As illustrated in Fig. 13a and Fig. 14a, TPMV decreases significantly when magnet width increases. Reason is that, by increase of magnet width, the magnet volume usage increases but torque does not increase accordingly, because magnet width increase does not affect principle harmonics of the machine. Therefore, magnet volume increases and TPMV decreases. However, changing magnet arc effects working harmonics of the machine. As a result, TPMV increases first but until arc is equal to 3.5 and 7 in CPDRVM-A and CPDRVM-B respectively. In this regard, PF value does not change considerably in correspondent with magnet width (Fig. 14a). PF is related to the magnet arc. Reason is that, since topology is a consequent pole, concentration of flux generated by magnets is affected considerably by magnet arc (Fig. 13a and Fig. 14a). Since magnet arc changes the cross section of core that is used by flux passing through. Thus, flux leakage decreases as magnet arc increases and higher PF achieved when magnet arc increases. Therefore, in order to find an optimized point both PF and TPMV should be considered.

Table V: overall comparison of machines

Parameter	PM	VM	DSSAVM	CPDRVM -A	CPDRVM -B
Torque (Nm)	120.3	520.43	1045.9	593.82	366.87
Magnet volume (cm^3)	807.3	888.05	1171.1	401.25	197.20
TPMV (Nm/cm^3)	0.208	0.58	0.89	1.479	1.85
PF	0.98	0.86	0.909	0.91	0.88
Copper loss (W)	26.5	26.5	16.53	37.66	36.49
Core loss (W)	2.22	16.79	43.07	17.61	11.79
Efficiency (%)	91	85	89	88	92

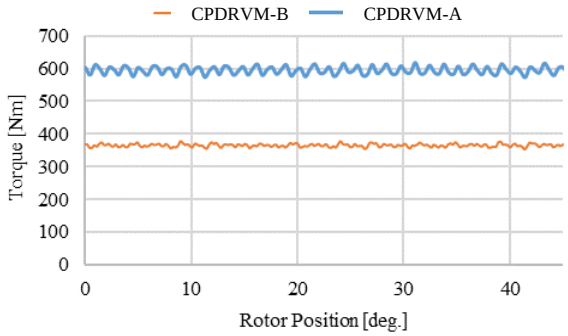

Fig. 15. Motor torque vs. rotor position in CPDRVM

B. *Performance discussion of proposed VMs*

Produced torque of the proposed CPDRVMs is illustrated in Fig. 15. The excitation current magnitude is considered 20 A in dual stator or rotor machines and 40 A in single stator machines. Table III demonstrates design values of the proposed CPDRVMs. These dimensions found out utilizing optimization and sensitivity analysis of the significant varaibles in Table I based on the constraints over PF and TPMV. Fig. 15 demonstrates that CPDRVM-B and CPDRVM-A have a very low torque ripple 8% and 6% respectively.

DSSAVM [15] utilized gamma angle in order to increase PF that also decreases generated torque. However, in this paper gamma angle which is angle between input current and Back-EMF considered to be zero.

Table V shows results of all analyzed machines, even though DSSAVM has highest torque value but in fair comparison regarding TPMV, proposed CPDRVM-A and CPDRVM-B produce 1.66 times and 2.07 times higher torque than DSSAVM respectively. In this regard, PF of CPDRVM-A (0.91) is almost same as PF of DSSA, 0.909. However, Model B has a lower PF, 0.88. In addition, CPDRVM-B has the lowest core loss, 11.79 Watts whereas core loss of CPDRVM-A and DSSA are 17.61 and 43.07 Watts respectively, which makes efficiency of them 88% and 89%. Therefore, among all machines CPDRVM-B has lowest core loss, highest TPMV and highest efficiency, which is 92 %.

VI. CONCLUSION

A novel structure of dual rotor vernier machine namely as CPDRVM, are introduced and investigated in this paper. This novel structure consisted of a stator that holds windings and inner and outer rotor that consisted of consequent pole magnets. In this regard, analytical design, electromagnetic analysis, sensitivity analysis and performance assessment are considered. In order to discover superiority of the proposed VM a comprehensive comparison with three typical machines, dual stator spoke array VM, single-sided VM and four-pole PM machine are considered. Significant properties that included in

this comparison are Back-EMF, magnet volume, TPMV, PF, losses, and efficiency. A reasonable comparison performed considering Back-EMF per magnet volume and TPMV, because magnet volume usage is not same in all machines. Obtained results indicate that TPMV of CPDRVM-A and CPDRVM-B is 1.66, 2.04 times higher than DSSAVM, and almost 2.6 times higher than Single-Sided VPM. In addition, PF of Model A and Model B are 0.91 and 0.88 respectively. Furthermore, sensitivity and optimization analysis show that proposed CPDRVMs could reach higher TPMV but with cost of lower PF and vice versa. Therefore, this is a tradeoff between torque production and PF. In addition, results show that between CPDRVM-B and DSSA, CPDRVM-B has highest TPMV and efficiency and lower torque ripple. Generally, the results show that proposed topologies have good potential to be used in various applications that requires lower magnet volume usage and consequently lower cost with high performance.

REFERENCES

[1] H. Torkaman, A. Ghaheri, A. Keyhani, "Design of Rotor Excited Axial Flux-Switching Permanent Magnet Machine," IEEE Transactions on Energy Conversion, vol. 33, no. 3, pp. 1175-1183, 2018.

[2] N. J. Baker, M. A. H. Raihan, A. Almoraya, J. Ji, H. Zhou, W. Zhou, T. Jiang, "A Cylindrical Linear Permanent Magnet Vernier Hybrid Machine for Wave Energy" IEEE Transactions on Energy Conversion, vol.34, no.2, pp. 691-700, 2019.

[3] H. Li, Z. Q. Zhu, "Optimal Number of Magnet Pieces of Flux Reversal Permanent Magnet Machines," IEEE Transactions on Energy Conversion, vol. 34, no. 2, pp. 889-898, 2019.

[4] H. Torkaman, A. Ghaheri, A. Keyhani,"Axial flux switched reluctance machines: a comprehensive review of design and topologies," IET Electric Power Applications, vol. 13, no. 3, pp. 310-321, 2019.

[5] E. Afjei, H. Torkaman, "Airgap eccentricity fault diagnosis in switched reluctance motor.", 1st Power Electronic & Drive Systems & Technologies Conference, Tehran, Iran, Feb., 2014, pp. 290-294.

[6] H. Torkaman, E. Afjei, "Magnetostatic field analysis and diagnosis of mixed eccentricity fault in switched reluctance motor," Electromagnetics, vol. 31, no. 5, pp. 368-383, 2011.

[7] H. Torkaman, N. Faraji, M. Toulabi, "Influence of Rotor Structure on Fault Diagnosis Indices in Two-Phase Switched Reluctance Motors," IEEE Transactions on Magnetics, vol. 50, no. 3, pp. 136-143, 2014.

[8] M. Cheng, P. Han, W. Hua, "General air-gap field modulation theory for electrical machines," IEEE Transactions on Industrial Electronics, vol. 64, no. 8, pp. 6063–6074, 2017.

[9] A. Arif, N. Baloch and B. Kwon, "Winding Switching and Turn Switching in Permanent Magnet Vernier Machines for Wide Speed Range Operation and High Efficiency," IEEE Access, vol. 7, pp. 55344-55357, 2019.

[10] J. Yu, C. Liu and H. Zhao, "Design and Multi-Mode Operation of Double-Stator Toroidal-Winding PM Vernier Machine for Wind-Photovoltaic Hybrid Generation System," IEEE Transactions on Magnetics, vol. 55, no. 7, pp. 1-7, 2019.

[11] X. Ren, D. Li, R. Qu, Z. Yu, Y. Gao "Investigation of Spoke Array Permanent Magnet Vernier Machine With Alternate Flux Bridges," IEEE Transactions on Energy Conversion, vol. 33, no. 4, pp. 2112 – 2121, 2018.

[12] T. Zou, D. Li, R. Qu, J. Li, D. Jiang "Analysis of a Dual-Rotor, Toroidal-Winding, Axial-Flux Vernier Permanent Magnet Machine" IEEE Transactions on Industry Applications, vol. 51, no. 4, pp. 1920–1930, 2015.

[13] S. Jia, R. Qu, J. Li, D. Lo, "Principles of Stator DC Winding Excited Vernier Reluctance Machines" IEEE Transactions on Energy Conversion vol. 31, no. 3, pp. 935 – 946, 2016.

[14] D. Li, R. Qu, W.Xu, J. Li, T. A. Lipo "Design procedure of dual-stator spoke-array Vernier permanent magnet machines." IEEE Transactions on Industry Applications, vol. 51, no. 4, pp. 2972–2983, 2015.

[15] D. Li, R. Qu, T. A. Lipo, "High power factor Vernier permanent magnet machines," IEEE Transactions on Industry Applications, vol. 50, no. 6, pp. 3664–3674, 2014.

[16] T. Zou, D. Li, C. Chen, R. Qu, D. Jiang, "A Multiple Working Harmonic PM Vernier Machine with Enhanced Flux-Modulation Effect" IEEE Transactions on Magnetics, vol. 54, no. 11, 2018.

[17] Y. Liu, H. Y. Li, Z. Q. Zhu, "A High-Power Factor Vernier Machine With Coil Pitch of Two Slot Pitches" IEEE Transactions on Magnetics, vol. 54, no. 11, 2018.

[18] J. Yu, C. Liu "Design of a Double-Stator Magnetless Vernier Machine for Direct-Drive Robotics", IEEE Transactions on Magnetics, vol. 54, no. 11, pp. 2972–2983, 2018.

[19] X. Zhao, S. Niu, W. Fu, "Torque Component Quantification and Design Guideline for Dual Permanent Magnet Vernier Machine" IEEE Transactions on Magnetics, vol.55, no.6, 2019.

[20] Q. Wang, S. Niu, T. Ching "A New Double-Winding Vernier Permanent Magnet Wind Power Generator for Hybrid AC/DC Microgrid Application" IEEE Transactions on Magnetics, vol. 54, no. 11, pp. 2972–2983, 2018.

[21] Z. Song, C. Liu, F. Chai and H. Zhao, "Modular Design of an Efficient Permanent Magnet Vernier Machine," IEEE Transactions on Magnetics, vol. 56, no. 2, pp. 1-6, 2020.

[22] L. Xu, G. Liu, W. Zhao, J. Ji, H. Zhou, W. Zhou, T. Jiang, "Quantitative Comparison of Integral and Fractional Slot Permanent Magnet Vernier Motors" IEEE Transactions on Energy Conversion, vol. 30, no. 4, pp. 1483 - 1495, 2015.

[23] J. W. Kwon, B. Kwon, "Investigation of Dual-Stator Spoke-Type Vernier Machine for EV Application," IEEE Transactions on Magnetics, vol. 54, no. 11, pp. 1-5, 2018.

[24] W. Liu, L. Sun, T. A. Lipo "On the Scaling of Consequent Pole Vernier Machines With Spoke Type Magnets" IEEE Energy Conversion Congress and Exposition, Portland, USA, Sept. 2018, pp. 3294-3301.

[25] Z. S. Du, T. A. Lipo, "High torque density ferrite permanent magnet vernier motor analysis and design with demagnetization consideration", IEEE Energy Conversion Congress and Exposition, Montreal, Canada, 2015, pp. 6082-6089.

[26] W. Liu, T. A. Lipo, "A family of vernier permanent magnet machines utilizing an alternating rotor leakage flux blocking design", IEEE Energy Conversion Congress and Exposition, USA, 2017, pp. 2461-2468.

[27] W. Zhao, A. Ma, J. Ji, X. Chen, T. Yao, "Multiobjective Optimization of a Double-Side Linear Vernier PM Motor Using Response Surface Method and Differential Evolution," IEEE Transactions on Industrial Electronics, vol. 67, no. 1, pp. 80-90, 2020.

[28] Q. Lin, S. Niu, W. Fu, "Design and Optimization of the Dual Permanent Magnet Vernier Machine with a Novel Optimization Model," IEEE Transactions on Magnetics. vol. 56, no. 3, 2020.

[29] L. Xu, W. Zhao, G. Liu and C. Song, "Design Optimization of a Spoke-Type Permanent-Magnet Vernier Machine for Torque Density and Power Factor Improvement," IEEE Transactions on Vehicular Technology, vol. 68, no. 4, pp. 3446-3456, 2019.